



Article

Evaluation of Suitable Habitats for Birds Based on MaxEnt and Google Earth Engine—A Case Study of *Baer's Pochard* (*Aythya baeri*) in Baiyangdian, China

Zengrui Tian ^{1,†}, Da Huo ^{1,†}, Kunpeng Yi ², Jialiang Que ¹, Zhenguang Lu ¹ and Jianhua Hou ^{1,*}

¹ College of Life Science, Hebei University, Baoding 071002, China; tianzengrui2022@163.com (Z.T.); hbuhuoda0509@163.com (D.H.); que2867068443@163.com (J.Q.); 15027927782@163.com (Z.L.)

² State Key Laboratory of Urban and Regional Ecology, Research Center for Eco-Environmental Sciences, Chinese Academy of Sciences, Beijing 100085, China; kpyi@rcees.ac.cn

* Correspondence: houjh@hbu.edu.cn

[†] These authors contributed equally to this work.

Abstract: The combined impacts of rapid urbanization and climate change pose significant threats to global biodiversity. To counter these threats, the establishment of appropriate habitats is becoming pivotal for species preservation. Due to positive ecological interventions, Baer's Pochard (*Aythya baeri*), a critically endangered avian species per the International Union for Conservation of Nature (IUCN) classification, has made a remarkable resurgence in the wetlands of Baiyangdian (BYD). BYD, located in Xiong'an New Area, central North China, is the largest wetland and an ideal habitat for rare bird species. Our study focuses on identifying ideal habitats within BYD to further its conservation. To this end, unmanned aerial vehicles (UAV) integrated with GPS functionalities were utilized to collect occurrence data for the species. Furthermore, the Google Earth Engine (GEE) provided access to high-resolution, real-time satellite imagery. Our model exhibited substantial reliability, reflected by area under the curve (AUC) values of 0.917 and 0.934 for breeding and migration periods, respectively. During the breeding phase, the prime habitat for Baer's Pochard spans 162 km², predominantly encompassing regions like Xiaobaiyangdian (XBYD), Zhaozadian (ZZD), Damaidian (DMD), and Shaochedian (SCD). Factors such as Distance to towns and Landcover predominantly influence breeding habitat selection. In the migration phase, ideal regions covered an expanse of 124 km², highlighting areas like northern and eastern SCD, the northwestern side of Datian Village (DTV) and Beitian Village (BTV) Fuhe Wetland (FHW), and Xiaoyihe Wetland (XYHW). The predominant determinants for migration habitat are Distance to towns and Wetness. These insights offer a fundamental foundation for the conservation and management strategies of Baer's Pochard in BYD, presenting a roadmap for future conservation endeavors.



Citation: Tian, Z.; Huo, D.; Yi, K.; Que, J.; Lu, Z.; Hou, J. Evaluation of Suitable Habitats for Birds Based on MaxEnt and Google Earth Engine—A Case Study of *Baer's Pochard* (*Aythya baeri*) in Baiyangdian, China. *Remote Sens.* **2024**, *16*, 64. <https://doi.org/10.3390/rs16010064>

Academic Editor: Melanie Vanderhoof

Received: 3 October 2023

Revised: 1 December 2023

Accepted: 6 December 2023

Published: 23 December 2023



Copyright: © 2023 by the authors. Licensee MDPI, Basel, Switzerland. This article is an open access article distributed under the terms and conditions of the Creative Commons Attribution (CC BY) license (<https://creativecommons.org/licenses/by/4.0/>).

Keywords: Baer's Pochard; suitable habitat area; MaxEnt; Google Earth Engine; conservation

1. Introduction

Rapid urbanization and environmental changes pose severe threats to biodiversity preservation [1,2]. On 1 April 2017, to alleviate non-capital functions from Beijing, the Chinese Government founded Xiong'an New Area. This area witnessed the implementation of several conservation-oriented policies aimed at fostering ecological development and preserving biodiversity [3]. While Xiong'an New Area has seen a surge in infrastructure development and urbanization, there has also been considerable ecological transformation, especially in the BYD wetlands. Historical research highlights that many recent artificial landscape constructions and ecosystem restoration efforts have not achieved the anticipated benefits, mainly due to a limited understanding of biologically suitable habitats [4–6]. Thus, pinpointing ideal habitat areas, especially for endangered species, is vital for efficient protected area planning and conservation strategy formulation [7,8]. This endeavor has

become pivotal in biodiversity conservation [9–11], offering an effective approach to species conservation. Species distribution models (SDMs) are increasingly acknowledged for their utility in mapping suitable habitats and ranges. Notable methods include CLIMEX, Genetic Algorithm for Rule Sets (GARP), and Maximum Entropy (MaxEnt) [12–15], with MaxEnt standing out due to its efficacy, even with sparse sample data [16–20]. The MaxEnt software, developed by Phillips, has become a pivotal analytical tool within species distribution modeling [21].

The Google Earth Engine (GEE, <https://earthengine.google.com/>, accessed on 7 December 2023) is a robust platform offering access to an extensive archive of long-term global satellite imagery and vector data, along with diverse processing tools, algorithms, and cloud-based computational resources [22]. This database includes imagery spanning over four decades, sourced from platforms like the Landsat series, the Moderate Resolution Imaging Spectroradiometer (MODIS), Sentinel “1, 2, 3”, among others. Moreover, it is augmented by datasets related to societal factors, demographics, topography, and climate [23]. Furthermore, GEE showcases substantial benefits over traditional techniques when processing time series multispectral satellite data [24,25]. By harnessing GEE’s autonomous algorithms and satellite image datasets, the quantification of habitats can yield a more immediate stream of real-time remote sensing data about vegetation. This offers a refined framework for exploring the intricate interplay between avian habitat selection and vegetation characteristics.

Baer’s Pochard (*Aythya baeri*), a water bird species in the Anatidae family, once spanned a vast territory ranging from Northeast Asia, through Southeast Asia, to the Indian subcontinent. According to the literature, during the breeding season, they primarily inhabited the Amur and Ussuri river basins in the Russian Far East and Northeast China. In the winter migration period, they were mainly observed in eastern and southern China, India, Bangladesh, and Myanmar [26]. Their diet primarily comprises aquatic plants like *Ceratophyllum demersum*, *Potamogeton crispus*, *Najas marina*, as well as tender leaves from plants like *Nelumbo nucifera*, *Typha orientalis*, and *Sagittaria trifolia*. Furthermore, they rely on aquatic invertebrates and insects adhering to aquatic stems and leaves [27]. Alarmingly, since 2008, the population of Baer’s Pochard has plummeted, leading the IUCN to categorize it as Critically Endangered. Estimates suggest the global population might be below 1000 [28,29]. Such a decline underscores the urgent need for concerted conservation efforts.

Earlier research employing the MaxEnt model primarily revolved around analyzing habitat distribution, assessing habitat suitability, and exploring habitat variation factors [30–32]. However, there is a research gap in using real-time environmental data on a granular scale, especially within the GEE framework. Baiyangdian (BYD), a significant habitat for Baer’s Pochard, is yet to be extensively investigated concerning the bird’s habitat preferences. Comprehensive studies on these habitats are not just pivotal for the bird’s conservation but also for strengthening BYD’s ecological dynamics [33]. The wintering range of waterfowl is linked to the extent of frozen-water cover, predominantly concentrated in unfrozen surfaces [34]. Accordingly, our research is centered on breeding and migration periods. The objectives of our study are as follows: (1) Identify Baer’s Pochard’s ideal breeding and migratory habitats in BYD; (2) examine the environmental determinants impacting habitat preferences; and (3) provide a reference to inform future habitat design, location specification, and eco-factor selection for the species.

2. Materials and Methods

2.1. Study Area

Baiyangdian (38°43′N to 38°49′N, 115°45′E to 116°07′E, Figure 1) is the largest freshwater lake and wetland in central North China, located in Hebei Province, China [35,36]. In addition, BYD has a temperate continental climate, with 143 lakes and more than 3700 trenches, covering an area of about 366 km² [37]. With the establishment of Xiong’an New Area, the ecological environment of BYD has been managed and protected. The water quality of the precipitation area is now in Class III and IV [38]. Class III is primarily applicable to wintering grounds

for fish and shrimp, migratory channels, and aquaculture areas. Class IV is mainly suitable for general industrial water and recreational water [39]. As a typical freshwater shallow lake-type wetland with unique natural landscapes, including waters, reed marshes, terrace fields, and lakeshore belts, BYD is an ideal habitat for many rare birds [40]. Protecting and improving the wetland environment of BYD has become an important part of the construction and development of Xiong'an New Area [41].

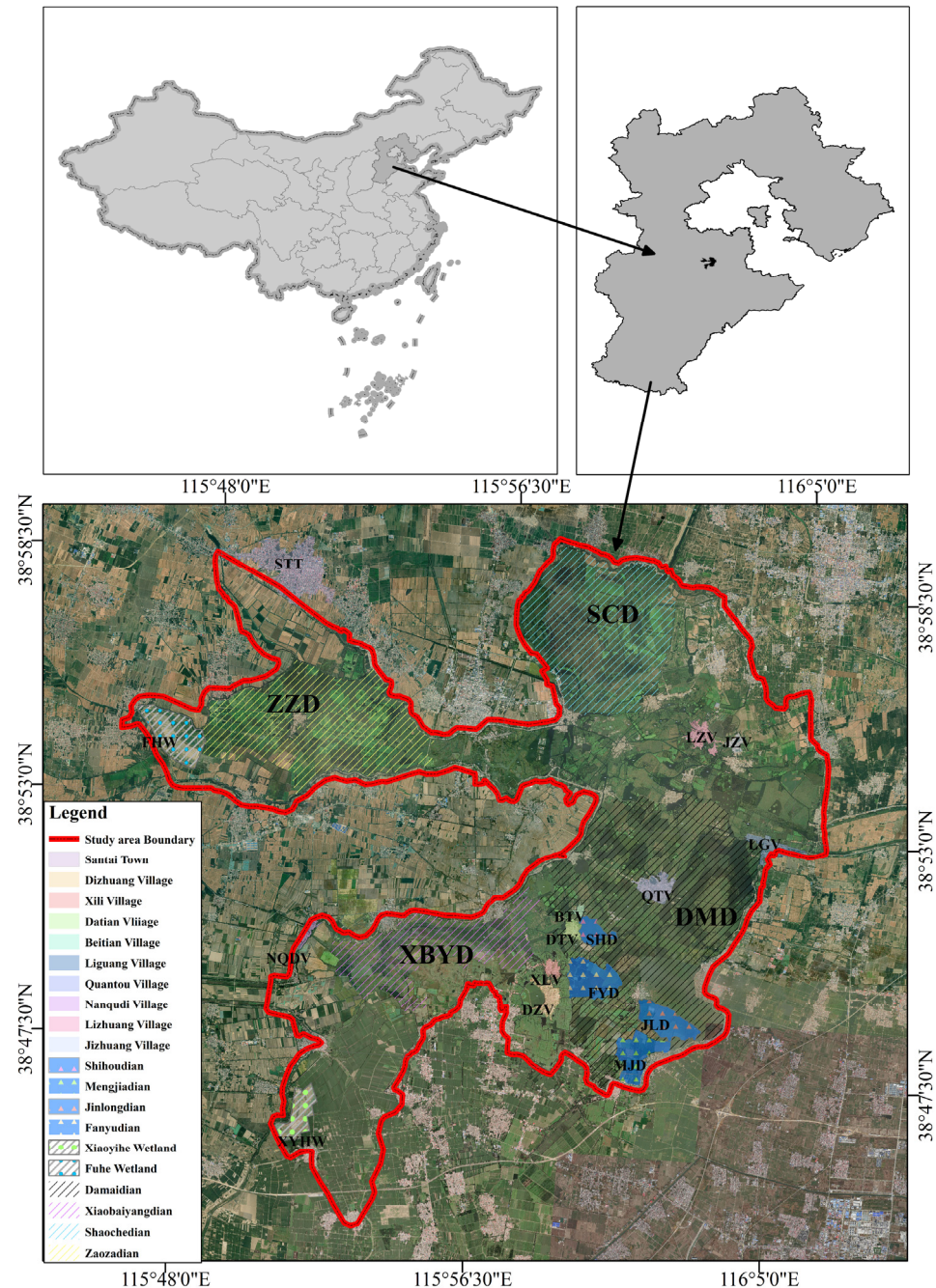


Figure 1. Geographical location of Baiyangdian. Baiyangdian, situated in Xiong'an New Area, Hebei Province, China, functions as a burgeoning breeding habitat for the Baer's Pochard. It ranks as the largest freshwater lake in North China, playing a pivotal role in the ecological development of Xiong'an New Area.

2.2. Acquisition of Occurrence Point Based on Field Surveys and Drone Monitoring

In our study, the occurrence points of Baer's Pochard were obtained during the breeding and migration periods (May–November 2022) through field surveys in BYD. A combination of the sample point method and sample line method was used to observe Baer's Pochard individuals using binoculars (Zeiss 10×), monoculars (Swarovski STX30-70 × 115), and a camera (7D, 100–400 mm). Using the GPS positioning function (horizontal: 1 cm + 1 ppm; vertical: 1.5 cm + 1 ppm) of the centimeter-level real-time kinematic (RTK) module mounted on the UAV (DJI Mavic 3 Enterprise), we located and photographed the target without disturbing the observation object, and collected data on the distribution of the individuals. A total of 78 points were observed during the breeding periods and 63 points during the migratory periods. To avoid overfitting, the occurrence points located within the same 10 m × 10 m grid cells were removed using the ENMtools base on ActivePerl (<https://www.activestate.com/products/perl/>, accessed on 7 December 2023) [42]. Finally, the occurrence points of 72 breeding periods and 49 migratory periods were obtained and converted into the csv form as required by MaxEnt 3.4 (https://biodiversityinformatics.amnh.org/open_source/maxent/, accessed on 7 December 2023).

2.3. Acquisition of Impact Factors Based on GEE

Based on previous studies and waterbird habitat selection behaviors [43–46], four aspects were considered: topography, environment, human impact, and climate.

A total of 42 impact factors were used to construct the model. The topographic factors were selected as Elevation, Aspect, and Slope. Normalized Difference Vegetation Index (NDVI), Enhanced Vegetation Index (EVI), Green Edge Normalized Difference Vegetation Index (GNDVI), Fractional Vegetation Cover (FVC), Index-based Built-up Index (IBI), Leaf Chlorophyll Index (LCI), Land Surface Water Index (LSWI), Optimization Soil-adjusted Vegetation Index (OSAVI), Modified Normalized Difference Water Index (MNDWI), Normalized Difference Built-up Index (NDBI), Normalized Difference Red Edge (NDRE), Landcover, Brightness, Wetness, and Greenness were selected as the environmental factors. Distance from roads, Distance from towns, Distance from water sources, Distance from water transportation, and Distance from fishing operation were selected as human-impact factors. Climate factors were extracted from WordClim, global climate and weather data (GEE only had access to v1 WordClim bioclimatic data), including Annual Mean Temperature, Mean Diurnal Range, Isothermality, Temperature Seasonality, Max Temperature of Warmest Month, Min Temperature of Coldest Month, Temperature Annual Range, Mean Temperature of Wettest Quarter, Mean Temperature of Driest Quarter, Mean Temperature of Warmest Quarter, Mean Temperature of Coldest Quarter, Annual Precipitation, Precipitation of Wettest Month, Precipitation of Driest Month, Precipitation Seasonality, Precipitation of Wettest Quarter, Precipitation of Driest Quarter, Precipitation of Warmest Quarter, Precipitation of Coldest Quarter.

Due to the acquisition time of occurrence points and the environmental variations between breeding and migratory periods, the environmental data were quantified by compiling Sentinel-2 satellite images taken between 23 May 2022 and 31 August 2022 as breeding satellite images, and those taken between 10 September 2022 and 31 November 2022 as migratory satellite images. All topography, environmental, and climate factors were obtained in GEE using the appropriate Java code. Using the random forest model of GEE, the Landcover of BYD was classified into five categories: town, water, agricultural/bare land, forest, and aquatic plant (Figure 2). Distribution data for roads, towns, water transportation, and fishing operations were obtained from field surveys, and corresponding distance impact factors were produced using the Euclidean Distance tool in ArcGIS 10.8 (<https://www.arcgis.com/index.html>, accessed on 7 December 2023) [47–49]. We extracted the water surface based on GEE during both the breeding and migratory periods. Then, we used the Euclidean Distance tool in ArcGIS 10.8 to calculate the distance to the water source for the two periods. Finally, all the impact factors were unified in ArcGIS 10.8 with a

raster size of 10×10 m; the unified coordinate system was WGS 1984. For the convenience of modeling, all impact factors, except Landcover, were reclassified in ArcGIS 10.8.

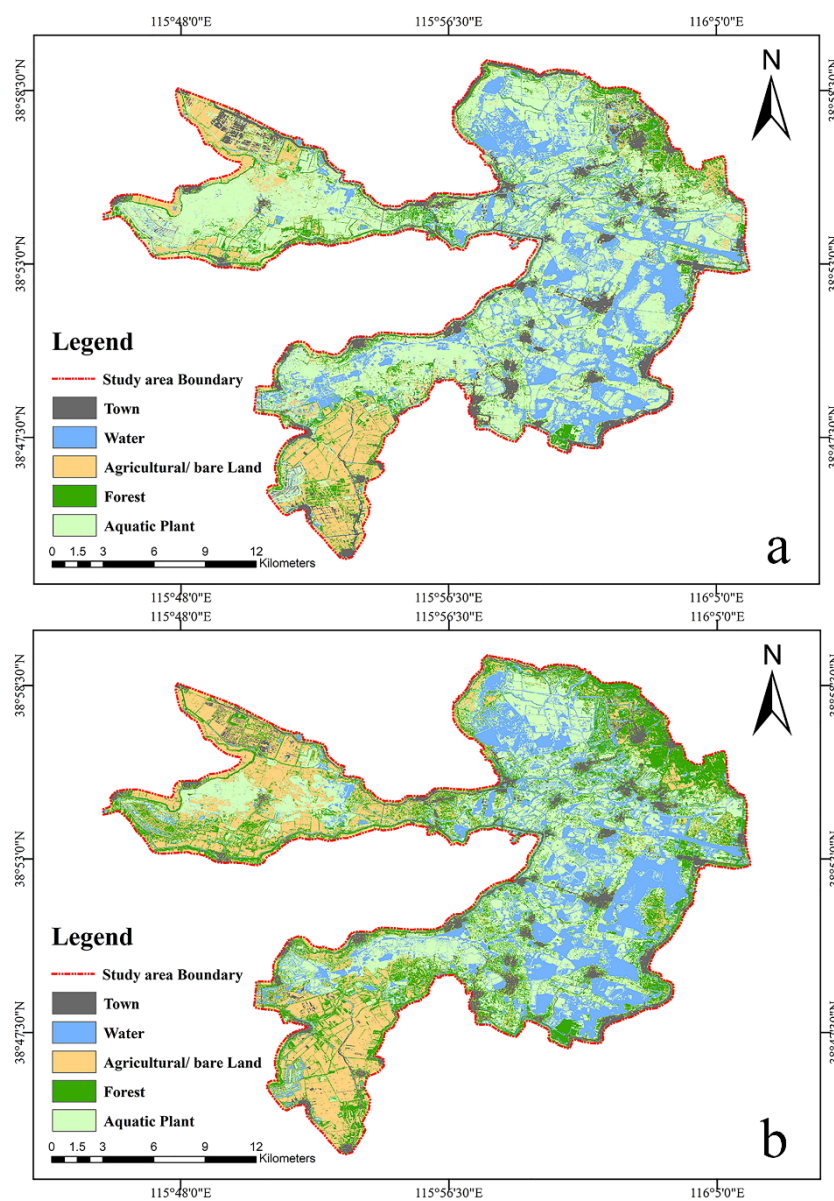


Figure 2. Landcover of Baiyangdian: (a) is the Landcover in breeding period; (b) is the Landcover in the migratory period. The black patch represents the town, the blue patch represents the water, the yellow patch represents the agricultural and bare land, the dark green patch represents the forest, and the light green patch represents the aquatic plants.

2.4. Screening of Impact Factors

To enhance model robustness and prevent overfitting, it is imperative to address the potential multicollinearity among environmental variables [50]. Multicollinearity can dilute the interpretability of individual predictors and inflate the standard errors of the coefficients. We utilized Pearson's correlation analysis in IBM SPSS (<https://www.ibm.com/cn-zh/spss>, accessed on 7 December 2023) to evaluate intercorrelations among the 42 impact factors for both breeding and migratory periods (Figure S1). Variables exhibiting a correlation magnitude ($|r|$) of 0.8 or greater were identified as highly correlated and subsequently excluded from the model [51]. The final set of environmental predictors, employed in modeling the probability of Baer's Pochard's occurrence during the breeding and migratory

periods after screening, is detailed in Table 1. This involves 22 factors for the breeding period and 20 factors for the migration period, selected from the original set of 42 factors.

Table 1. Impact factors screened for modeling the selection of suitable habitats for Baer’s Pochard during breeding and migratory periods.

| Type | Variables | Period | Unit |
|--------------------------|--|--------------------|------|
| Topographic Factors | Elevation | Breeding/Migratory | m |
| | Slope | Breeding/Migratory | ° |
| | Aspect | Breeding/Migratory | ° |
| Environmental Factors | Fractional Vegetation Cover (FVC) | Breeding/Migratory | — |
| | Landcover | Breeding/Migratory | — |
| | Modified Normalized Difference Water Index (MNDWI) | Breeding/Migratory | — |
| | Normalized Difference Built-up Index (NDBI) | Migratory | — |
| | Wetness | Breeding | — |
| Human-impact Factors | Eucdist to Town | Breeding/Migratory | Km |
| | Eucdist to Road | Breeding/Migratory | Km |
| | Eucdist to Water | Breeding/Migratory | Km |
| | Eucdist to Water Transportation | Breeding/Migratory | Km |
| | Eucdist to Fishing Operations | Breeding/Migratory | Km |
| Climatic Factors | Annual Mean Temperature | Breeding/Migratory | °C |
| | Isothermality | Breeding/Migratory | — |
| | Mean Diurnal Range | Breeding | °C |
| | Max Temperature of Warmest Month | Breeding | °C |
| | Min Temperature of Coldest Month | Breeding | °C |
| | Mean Temperature of Warmest Quarter | Breeding/Migratory | °C |
| | Mean Temperature of Coldest Quarter | Breeding/Migratory | °C |
| | Precipitation Seasonality | Breeding/Migratory | mm |
| | Precipitation of Driest Month | Migratory | mm |
| | Precipitation of Coldest Quarter | Breeding | mm |
| | Precipitation of Warmest Quarter | Migratory | mm |
| | Precipitation of Wettest Quarter | Breeding | mm |
| Temperature Annual Range | Migratory | — | |

2.5. Species Distribution Modeling and Evaluation

Feature Combinations (FC) and the Regularization Multiplier (RM) have considerable influence on the simulated outcomes within the MaxEnt model [52,53]. Diverse parameter combinations give rise to models of distinct complexity. In our study, model optimization was executed through the utilization of the ENMevaluate function from the ENMeval package in R [54]. The RM factors, ranging from 0.5 to 4 in intervals of 0.5, were systematically combined with FC that include L (linear), LQ (linear, quadratic), LQH (linear, quadratic, hinge), H (hinge), LQHP (linear, quadratic, hinge, product), and LQHPT (linear, quadratic, hinge, product, threshold) [55]. Subsequently, the resulting 48 combinations underwent parameter tuning facilitated by the ENMeval package. The optimal parameter combination, determined by selecting delta. AICc = 0 was then chosen for subsequent MaxEnt modeling [56,57]. We partitioned our dataset with 75% of the occurrence points forming the training set for modeling, and the remaining 25% allocated as a test set for validation [58]. Based on the results of MaxEnt model optimization, the parameter combinations for RM and FC during the breeding and migration periods were established, respectively. The MaxEnt model underwent 10 replicate runs, each with a cap of 500 iterations. Jack-knife tests and cross-validation were applied to gauge the relative importance of individual environmental factors. The output was set to Logistic mode, keeping other parameters at default.

For assessing the predictive outcomes, this study employed the Area Under Curve (AUC) of the receiver operating characteristic (ROC) curve to evaluate accuracy [59]. The AUC value, ranging from 0 to 1, commonly indicates the precision of the model’s predictive

outcomes. The evaluation criteria are as follows: AUC values within the range of 0.9 to 1.0 excellent, 0.8–0.9 = good, 0.7–0.8 = average, 0.6–0.7 = poor, and 0.5–0.6 = insufficient [60,61].

The MaxEnt logistic output format, having values between 0 and 1, was further processed using ArcGIS 10.8. We applied the Maximum Test Sensitivity Plus Specificity (MTSPS) thresholding method for reclassification [62–64]. Grid cells with logistic suitability values above this threshold were flagged as suitable habitats. Drawing from previous studies [65–67], these suitable habitats were tiered into the following: high suitability (0.6–1), moderate suitability (0.4–0.6), and low suitability (MTSPS-0.4).

2.6. Technical Workflow Overview

Our study is structured into three distinct stages: the acquisition of Baer’s Pochard occurrence data and relevant impact factors, the construction of the MaxEnt model, and the review of model results for the identification of protected areas (Figure 3).

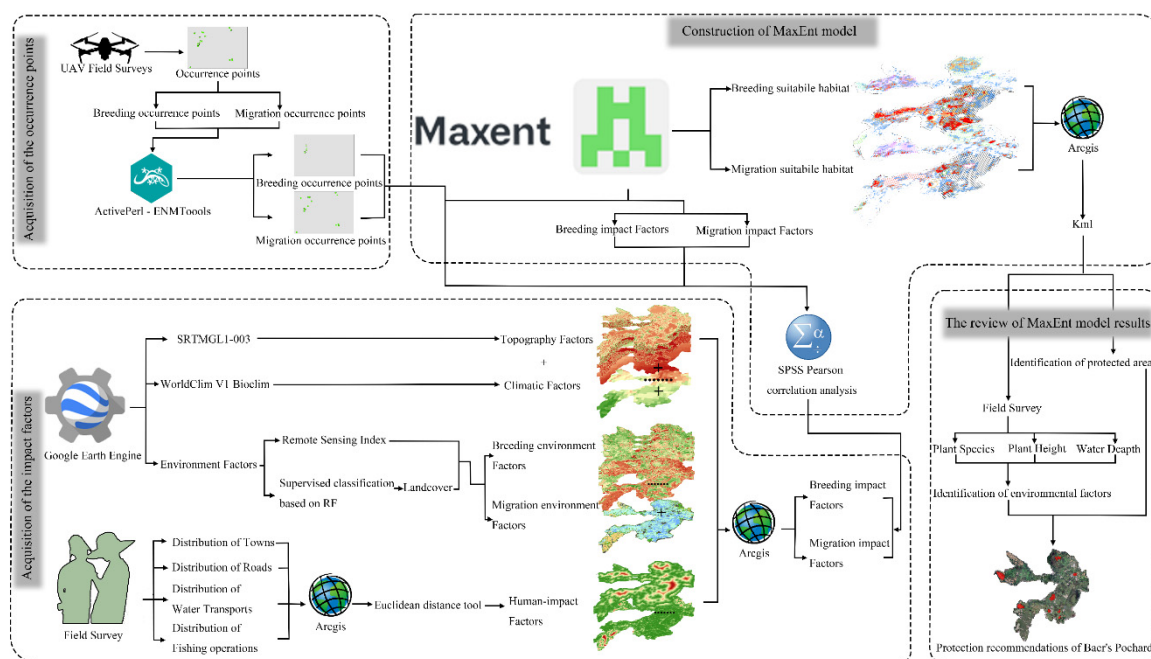


Figure 3. Flow chart for the identification of habitat suitability for Baer’s Pochard.

In the initial section, an unmanned aerial vehicle (UAV) equipped with a centimeter-level real-time kinematic (RTK) module for precise GPS positioning was employed. Positioned directly above the target at an altitude of 50 m, highly accurate occurrence points of Baer’s Pochard were acquired. This method resulted in species coordinates precise to eight decimal places, meeting the 10 m × 10 m prerequisites for impact factors in the MaxEnt model. Data collection encompassed four facets: topography, environment, human impact, and climate. Topography and climate factors had dedicated databases in the GEE, easily integrated into the MaxEnt model after straightforward processing. Environmental factors were quantified using Sentinel-2 imageries from the GEE database. To enhance research reliability, various remote sensing indexes reflecting environmental fluctuations were employed. Additionally, a supervised classification based on the random forest model was utilized to delineate landcover during the breeding and migration phases of Baer’s Pochard in BYD. Extensive field surveys conducted over several years documented the distribution of towns, roads, water transport, and fishing operation within BYD. Using the Euclidean distance tool in ArcGIS 10.8, representative impact factors representing the distances between the entirety of BYD and various anthropogenic disturbances were formulated.

In the subsequent section, Baer’s Pochard occurrence data and impact factors from the first segment were processed. Time-based segmentation into breeding and migration periods was conducted using temporal information derived from the occurrence data. To prevent overfitting, ENMTools was utilized to handle occurrence data from different periods, excluding points co-located within the same 10 m × 10 m grid. The coordinate system for all factors was standardized to WGS 1984, and the grid size was set to 10 m × 10 m using ArcGIS 10.8. Furthermore, impact factors were reclassified to streamline model computations. Potential collinearity among factors was addressed through Pearson correlation analysis, leading to the exclusion of factors with a correlation $|r| \geq 0.8$. In the end, the filtered occurrence data points and impact factors were imported into the MaxEnt software to construct the species distribution model. Regarding MaxEnt parameters, 75% of the distribution points were utilized for the training set, with the remaining 25% reserved as a test set. The model underwent 10 repetitions with a maximum iteration count of 500. The relative contributions of each environmental variable were assessed using the jackknife method, and the selected output type was the Logistic model, with all other parameters set to their default values.

In the third section, the results obtained from the MaxEnt model, as described in the second section, were revisited. The segments of moderate and high suitability habitats from the distribution maps of Baer’s Pochard during the breeding and migration periods were isolated and exported as KML files to aid field investigators in precisely locating survey areas. By comparing two KML files, priority was given to revisiting overlapping regions, and a proposal was made to designate the spatial extent with high suitability for Baer’s Pochard during both breeding and migration periods as a dedicated protected area. Throughout the revisiting survey, documentation of plant species, height, and water depth within the KML file ranges occurred, contributing to a more nuanced understanding of Baer’s Pochard habitat preferences. The details from the third section are incorporated into the discussion.

3. Results

3.1. Evaluation of MaxEnt Model Optimization and Results

Using the ENMeval package, we conducted a cross-validation optimization of the MaxEnt model based on the occurrence points and impact factors of Baer’s Pochard at different periods, considering various combinations of RM and FC. In accordance with the optimization outcomes (Figure S2), a value of 1.5 was opted for RM and Hinge functions for FC during the breeding period, while a value of 2.5 was selected for RM and Hinge for FC throughout the migration period. Comparative results with default parameters showed a 4.4% decrease in AICc and a significant 45.5% reduction in Mean.OR₁₀ during the breeding period. Similarly, there was a 3.8% decrease in AICc, accompanied by a 36.4% reduction in Mean.OR₁₀ during the migration period (Table 2). These results demonstrate that, whether during the breeding or migration period, model optimization led to a reduction in both model complexity and overfitting, leading to enhanced model accuracy.

Table 2. Evaluation metrics of MaxEnt model generated by ENMeval.

| Period | Parameter Settings | Regularization Multiplier | Feature Combinations | AICc | Delta.AICc | Mean.OR ₁₀ |
|------------------|--------------------|---------------------------|----------------------|---------|------------|-----------------------|
| Breeding Period | Default | 1 | LQHP | 2272.73 | 99.89 | 0.31 |
| | Optimized | 1.5 | H | 2172.83 | 0 | 0.17 |
| Migration Period | Default | 1 | LQHP | 1501.64 | 56.46 | 0.23 |
| | Optimized | 2.5 | H | 1445.18 | 0 | 0.15 |

The MaxEnt model’s effectiveness was evaluated by observing the AUC values for both the breeding and migration seasons. The breeding season model performance was robust, reflected by its commendable AUC values. The AUC, representing the ability of

the model to distinguish between presence and absence areas, scored an average of 0.917 during the testing phase after 10 iterations of cross-validation. The average training AUC, showcasing the model's inherent fitting to the provided data, was higher at 0.942. This high AUC range (see Figure 4a) signifies that the model achieved an excellent performance in predicting the suitable habitats for Baer's Pochard during its breeding period. The model's performance during the migration season was even more impressive. The testing phase scored an average AUC of 0.934, while the training phase achieved an average of 0.955. These numbers, as visualized in Figure 4b, depict an outstanding ability of the model to accurately pinpoint suitable habitats for Baer's Pochard during their migration.

Average Sensitivity vs. 1-Specificity for *Aythya baeri*.

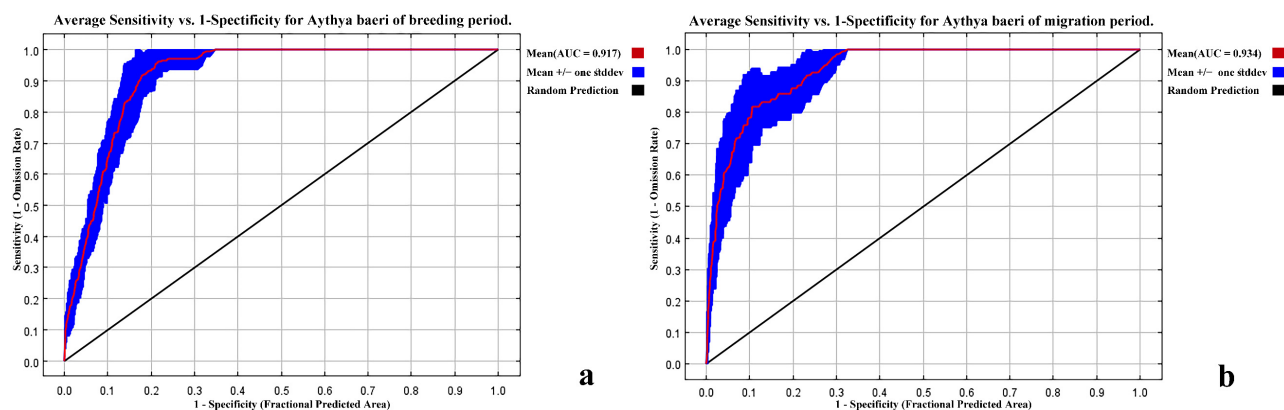


Figure 4. AUC curves for modeling habitat suitability of Baer's Pochard: (a) is the AUC curves for Baer's Pochard of breeding period; (b) is the AUC curves for Baer's Pochard of migration period. The red (test) line represents the average fit of the model to the training data. The blue area represents the standard deviation of the fit of the model to the test data.

The AUC values are an industry-standard metric for model performance, with values nearing 1 denoting perfect accuracy. For both the breeding and migratory seasons, the obtained AUC values are notably high. This means that the MaxEnt model was exceptionally efficient in predicting suitable habitats for Baer's Pochard in BYD. Given these AUC scores, stakeholders can place a high degree of confidence in the model's predictions. This robustness in prediction will prove vital in conservation efforts and habitat management for Baer's Pochard in BYD.

3.2. Relationship between the Selection of Suitable Habitat Areas and Impact Factors

Our outcomes of the MaxEnt revealed that, based on the jack-knife test utilizing individual impact factors, Wetness (1.1884), MNDWI (1.1395), Distance to town (1.0918), Landcover (1.0792), Elevation (1.0715), and Distance to water (1.063) ranked higher in terms of their regularization test gains for suitable habitat of Baer's Pochard during the breeding period (Figure S3a). Among the refined set of 22 environmental variables, Distance to town, MNDWI, Wetness, Landcover, Distance to water transport, and Distance to water exerted greater influences on the potentially suitable areas for the breeding period, contributing to an accumulated percentage of 95.48% and cumulative importance of 82.47% (Figure S3b). The analysis reveals that among various impact factors, Distance to town, Distance to water, MNDWI, Wetness, and Landcover stand out consistently in both the individual environmental variable jack-knife tests and their contribution to overall factor significance, underscoring their influential role in suitable habitat determination (Figure S3).

Detailed assessments indicate that optimal breeding habitats for Baer's Pochard are characterized by a higher probability of distribution within the 0.2–1.4 km range from the town, with the peak probability occurring between 0.39 km and 0.45 km. In the proximity of water transport, the probability of distribution is elevated within the 0.8–7.3 km range, reaching its maximum between 2 km and 2.3 km. The distribution probability diminishes

with an increasing distance from open water, being more pronounced within distances less than 167.7 km. As the MNDWI increases, the distribution probability also increases, with a higher probability observed when MNDWI is greater than -0.16 and reaching its zenith when MNDWI exceeds 0.29 . The probability initiates an upward trend when Wetness surpasses -0.13 , is more prominent when exceeding -0.01 , and reaches its pinnacle when surpassing 0.13 . Areas characterized by aquatic vegetation exhibit the highest distribution probabilities (Figure S4).

The MaxEnt results of the migratory period demonstrated that, based on individual environmental variables assessed through jack-knife tests, MNDWI (1.2429), Distance to town (1.1897), Distance to water (0.9857), Elevation (0.958), NDBI (0.9423), and Slope (0.9385) rank higher in terms of their regularization test gains for suitable habitats for Baer's Pochard (Figure S5a). Among the refined set of 20 impact factors, Distance to town, MNDWI, Distance to road, Distance to fishing operations, Mean Temperature of Coldest Quarter, and Distance to water exerted greater influences on the potential suitable areas for migratory period, contributing to an accumulated percentage of 96.03% and cumulative importance of 95.34% (Figure S5b). For the migratory period, Distance to town, Distance to water, and MNDWI predominantly influence habitat choice, reflected in individual environmental variable jack-knife tests and their total factor significance (Figure S5).

Suitable habitats for Baer's Pochard during migration likely exhibit an elevated distribution probability at distances exceeding 0.16 km from the town, reaching a peak within the 0.4–0.5 km range. The likelihood of distribution increases proportionally with the distance from fishing operations, reaching its peak at 1.40 km and maintaining a consistent level thereafter. In contrast, the distribution probability diminishes as the distance from open water increases, particularly within distances of less than 0.17 km. Additionally, the distribution probability decreases as the distance from roads increases, with a significant probability within the range of 1.13 km from the road. Furthermore, the distribution probability increases with an increase in FVC, peaking within the FVC range of 0.67–0.76. Moreover, the distribution probability increases with the increase in MNDWI, particularly when MNDWI exceeds -0.16 and reaches its maximum between -0.02 and -0.01 (Figure S6).

3.3. Spatial Patterns of Suitable Habitats for Baer's Pochard

For the breeding season, the total suitable habitat area spans 162.39 km^2 . Additionally, the area of low-suitability habitat is 65.35 km^2 , the moderate-suitability habitat covers an area of 69.12 km^2 , and the high-suitability habitat occupies 27.92 km^2 (Table S1). In terms of spatial distribution, the high-suitability breeding habitat primarily spans the regions of XBYD, Jinlongdian (JLD), Mengjiadian (MJD), Shihoudian (SHD), Fanyudian (FYD), west of Dizhuang Village (DZV), west of DTV, and north of BTV. The moderate-suitability habitat is mainly distributed on the SCD, along the shores of northern and western parts of the central region within the lake, as well as the east of DMD and the northeast and northwest sides of Quantou Village (QTV). The low-suitability habitat is extensively distributed across ZZD, the south of XBYD, and the north of DMD, while also being scattered throughout the southeast of Santai Town (STT), east and west sides of the Baiyangdian Grand Bridge, east of Jizhuang Village (JZV), west and south of Lizhuang Village (LZV), and north of Liguang Village (LGV) (Figure 5a).

For the migratory season, the suitable habitat stretches over 124.44 km^2 . The low-suitability habitat covers an area of 48.02 km^2 , the moderate-suitability habitat spans 52.9 km^2 , the high-suitability habitat area measures 23.52 km^2 (Table S2). Regarding spatial distribution, the high-suitability migratory habitat is scattered in various regions, including the northern and eastern sides of SCD, western and southern sides of ZZD, FHW, the northwestern side of DTV and BTV, southeast side of Nanqudi Village (NQDV), XYHW, areas west of DZV, MJD, and north of JZV. The moderate-suitability habitat is primarily identified within the SCD, predominantly in its central section, featuring expansive regions to the north and southwest. Furthermore, it is observed in the northwestern sector of the MJD, the central area of the XBYD, and the southern part of the LZV. The low-suitability

habitat is primarily fragmented within the DMD and ZZZ regions, predominantly situated in the peripheral areas of medium-suitability habitat (Figure 5b).

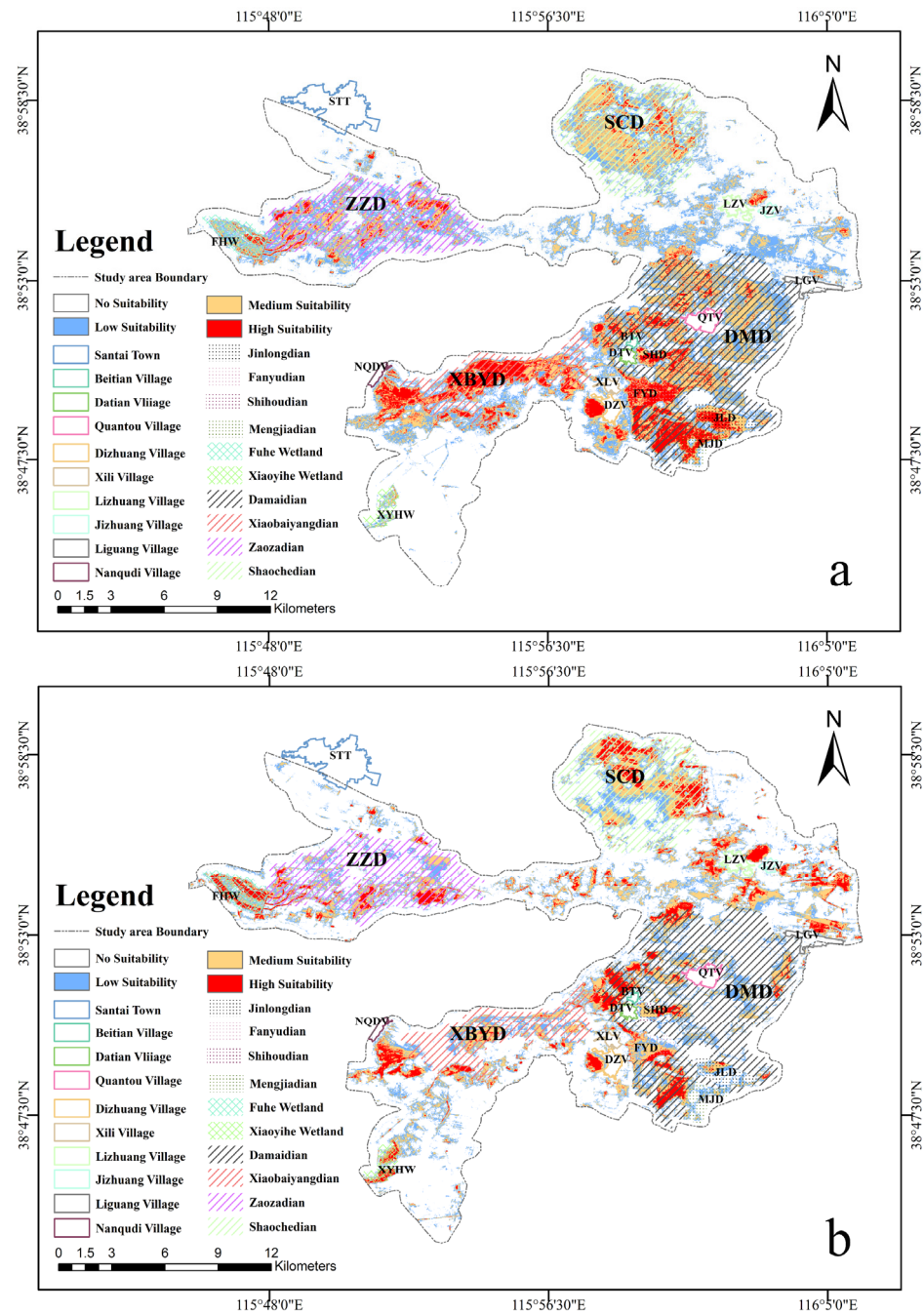


Figure 5. Map of suitable habitats for Baer’s Pochard in the study area: (a) shows the breeding suitable habitats; (b) shows the migration suitable habitats. The white patch represents the unsuitable habitats, the blue patch represents the low-suitability habitats, the yellow patch represents the moderate-suitability habitats, and the red patch represents the high-suitability habitats).

3.4. Seasonal Changes in Suitable Habitat Areas for Baer’s Pochard

The migratory season witnesses a 37.95 km² decline in suitable habitat areas compared to the breeding season. This reduction encompasses changes across all suitability categories: high (−4.4 km²), moderate (−16.22 km²), and low (−17.33 km²).

Contrasting with the breeding season, the migratory high-suitability habitat expanded by 15.19 km², contracted by 19.41 km², and remained unchanged in an area of 7.17 km².

In comparison with the breeding season, the expanded high-suitability habitat during the migration period was mainly located in the northern and northeastern regions of FHW, XYHW, SCD, and the northwest portions of DTV and BTV. Contrarily, the contracted areas were primarily situated in the central parts of XBYD, JLD, NJD, and FYD (Figure 6a). The moderately suitable habitat saw an expansion of 31.33 km², a contraction of 46.73 km², and an unchanged area of 18.94 km². The expanded moderate-suitability habitat was concentrated in the central parts of XBYD, the eastern regions of SCD, FYD, and LZV. Conversely, the contracted areas were predominantly found in the southeast of FHW, NQDV, the western and southern regions of SCD, and DMD (Figure 6b). In the low-suitability habitat, there was an expansion of 33.76 km², a contraction of 50.24 km², and an unchanged area of 11.89 km². The expanded low-suitability habitat was observed in XBYD, the central areas of SCD, FYD, and JLD, while contraction occurred in FHW, XYHW, DMD, SCD, and the southern parts of XBYD (Figure 6c).

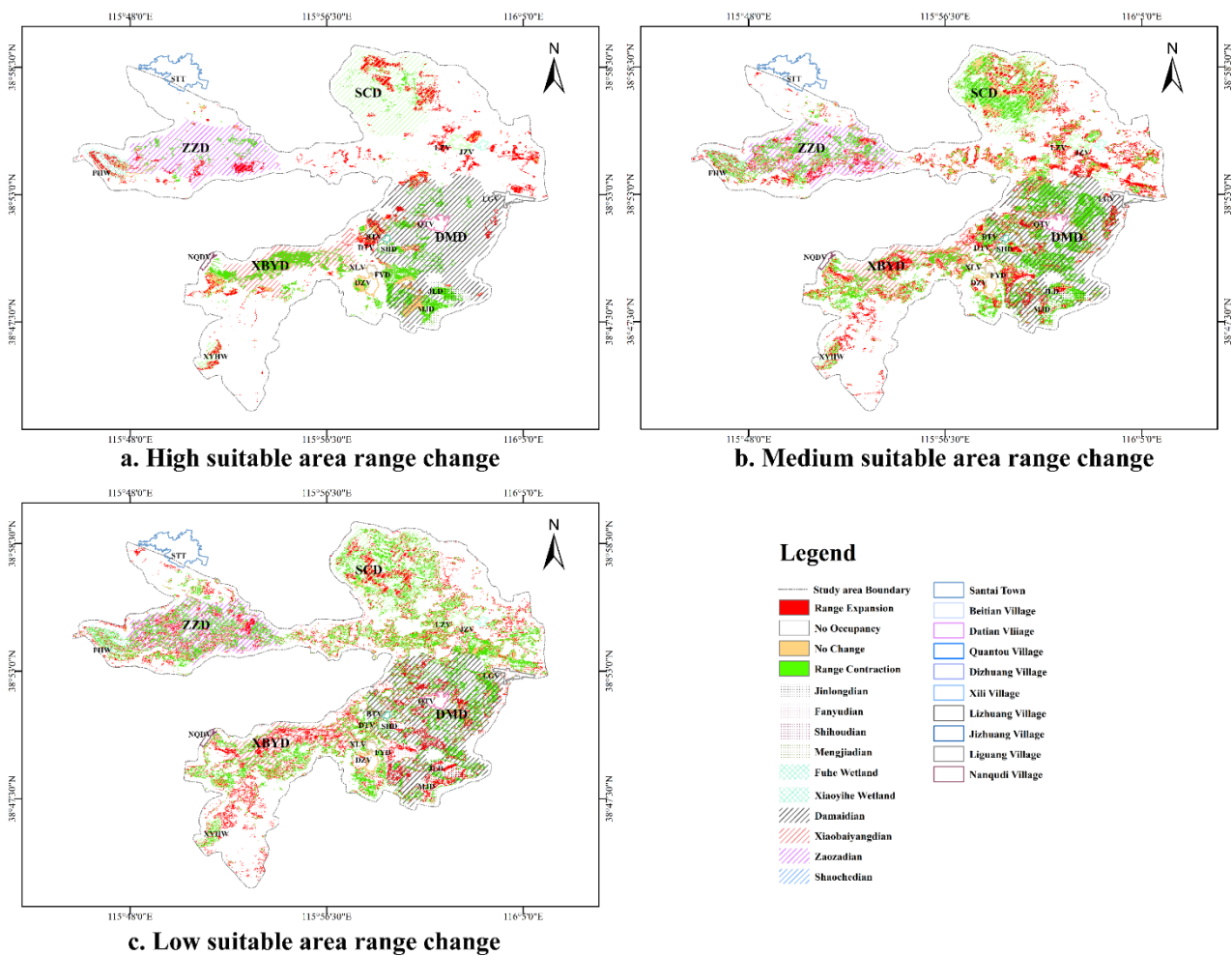


Figure 6. Changes in suitable areas for Baer’s Pochard in the study area: (a) shows the seasonal variation in the high-suitability habitat, (b) shows the seasonal variation in the moderate-suitability habitat, and (c) shows the seasonal variation in the low-suitability habitat.

4. Discussion

As the ecological environment in BYD improves, more bird species, including the critically endangered Baer’s Pochard, are turning to it for breeding, stopover, and wintering. Only unfrozen water surfaces are particularly attractive to waterfowl during the wintering period, hence our focus on breeding and migratory seasons. In prior MaxEnt-based habitat studies [30,32], researchers commonly opted for broader spatial scales. However, BYD exhibits a relatively diminutive area, and the methodologies in previous investigations for

acquiring occurrence points and impact factors were hampered by precision constraints, falling short of achieving the anticipated outcomes. This underscores the necessity for enhanced precision in determining the distribution points of Baer's Pochard and a heightened resolution for environmental factors. In addressing these requisites, we deployed a UAV equipped with a centimeter-level RTK module for GPS positioning. The UAV was strategically positioned directly above Baer's Pochard to acquire distribution points with exceptional accuracy. Moreover, to satisfy the elevated resolution and temporal demands of impact factors, we employed the GEE platform. GEE excels in concurrently processing substantial volumes of remote sensing data, facilitating expeditious image processing and analysis. Conventional tools may encounter constraints in computational resources, particularly when handling extensive satellite imagery, potentially leading to protracted processing times. Additionally, GEE offers real-time access to an extensive collection of satellite imagery. Users can promptly retrieve the latest satellite images from the GEE platform, facilitating real-time monitoring and applications. Conversely, traditional methods may necessitate more time and resources to acquire the most recent satellite imagery, involving manual downloading, processing, and managing extensive datasets [68,69].

We aimed to outline an approach for providing a novel outlook on exploring seasonal changes in waterbird habitat preferences within a localized area. Specifically, our innovative approach involved the use of GEE to obtain impact factors, a methodology unprecedented in previous research on the habitat suitability of Baer's Pochard [45,46]. We anticipate that the application of this interdisciplinary tool will aid in producing more accurate simulation results for species distribution models. The widespread adoption of this methodology can provide a more convenient approach to acquiring impact factors for future studies into species habitat suitability within localized regions. Moreover, we explored the effects of combining RM and FC parameters on MaxEnt results, optimizing the parameter combination of the MaxEnt model with the ENMTools tool. Significant reductions in AICc and Mean.OR₁₀ were observed compared to the default parameter combination, indicating reduced model complexity and overfitting, ultimately enhancing model accuracy. This consideration represents an aspect overlooked in prior studies on Baer's Pochard habitat suitability [70]. However, we acknowledge certain limitations in our study. The Landcover factor, created through a random forest model, faces constraints due to the precision of Sentinel-2 imagery, permitting the classification of factors into only five subcategories. To further investigate the impact of landcover on species habitat selection in a confined region, employing higher-precision satellite imagery or UAV orthophotos to define additional habitat types would enrich the study. Additionally, acquiring more direct climate variable data poses challenges and relies on the WorldClim dataset. Given its lower resolution, this dataset may not precisely capture temperature and precipitation variations in specific localized areas of BYD, such as ponds, towns, and villages.

Our findings underscored the significance of factors like Distance to town, Distance to water, and MNDWI in determining suitable habitats during both the breeding and migratory periods. Baer's Pochard is more likely to be found within the spatial range from 0.39 km to 0.50 km from towns, from 2 km to 2.3 km from water transport, greater than 1.40 km from fishing operations, less than 0.17 km from open-water surfaces, and less than 1.13 km from roads. Additionally, within these areas, the probability of detection is higher when the MNDWI is greater than 0.29 and Wetness is greater than 0.13 during the months of May to August. In the period from September to November, MNDWI typically ranges from −0.02 to 0.01, and vegetation coverage falls within the range from 0.67 to 0.76. Generally, regions with higher MNDWI and Wetness values, ecologically, may signify richer aquatic ecosystems, offering more ecological niches and resources to support diverse biological communities [71,72].

Field surveys were carried out in the medium- and high-suitability habitat zones identified through MaxEnt modeling, and plant species present in these areas were documented. The survey results reveal a preference for reed-enclosed paddy fields, particularly in marshy fields and ponds with *Nelumbo nucifera* (0.3–0.6 m) and *Potamogeton crispus* growth (as visualized in Figure 7). Some locations also feature *Populus L.* (16–22 m) with varied heights

depending on their location. Moreover, water depths in the region predominantly range from 1.5 m to 2.5 m. Figures 5 and 6 offer geographic insights into Baer's Pochard habitat suitability, while Figure 8 provides a schematic view of their suitable habitats. These habitats are primed for the foraging needs of Baer's Pochard and offer protection from predators. Our findings indicate that the Distance to towns is not the sole determinant of their distribution; habitats like enclosed paddy fields with *Nelumbo nucifera* or *Potamogeton crispus* are pivotal for Baer's Pochard. Our study confirms that Baer's Pochard does not typically favor open-water habitats. Perhaps these habitats better fulfill the foraging and predator avoidance needs of Baer's Pochard. During migration, suitable habitats, especially high-suitability habitats, shift to FHW, XYHW, and the northwestern side of DTV. This may be attributed to the vegetation dynamics within the originally suitable area during the migration period, hindering Baer's Pochard from effectively evading predators and foraging. As a result, they tend to be concentrated in reed-enclosed paddy fields with *Nelumbo nucifera* growth, such as FHW and XYHW. The suitable habitat area for Baer's Pochard undergoes a substantial reduction during migration, in contrast to the breeding season. This observation concurs with the documented phenomenon of Baer's Pochard exhibiting a southward migration pattern in response to seasonal changes in China, as elucidated by Liu et al. [46]. Based on the MaxEnt results, we propose establishing specific zones for the effective conservation of Baer's Pochard (as depicted in Figure 9). Within these designated conservation areas, we advise maintaining water depths within the range of 1.5–2.5 m, with *Phragmites australis* reaching a height of 2–3.6 m and *Nelumbo nucifera* at a height of 0.2–0.6 m. Furthermore, to align with Baer's Pochard's dietary preferences, the supplementary planting of vegetation like *Potamogeton crispus* and *Typha orientalis* could be advantageous [27].

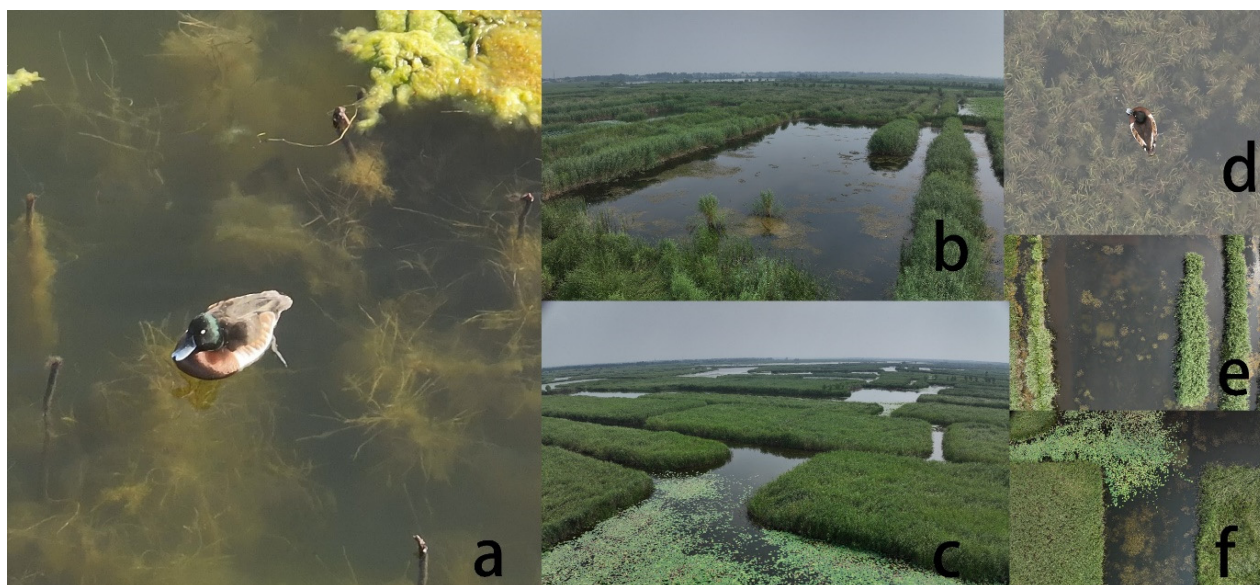


Figure 7. Photographs of Baer's Pochard species and habitats: (a) shows a species photograph of the Baer's Pochard; (b,c,e,f) are aerial photographs of the distributional habitats of Baer's Pochard and the corresponding aerial orthophotos at an altitude of 50 m; and (d) shows the *Potamogeton crispus* that Baer's Pochard feeds on.



Figure 8. Schematic diagram of suitable habitat for Baer's Pochard.

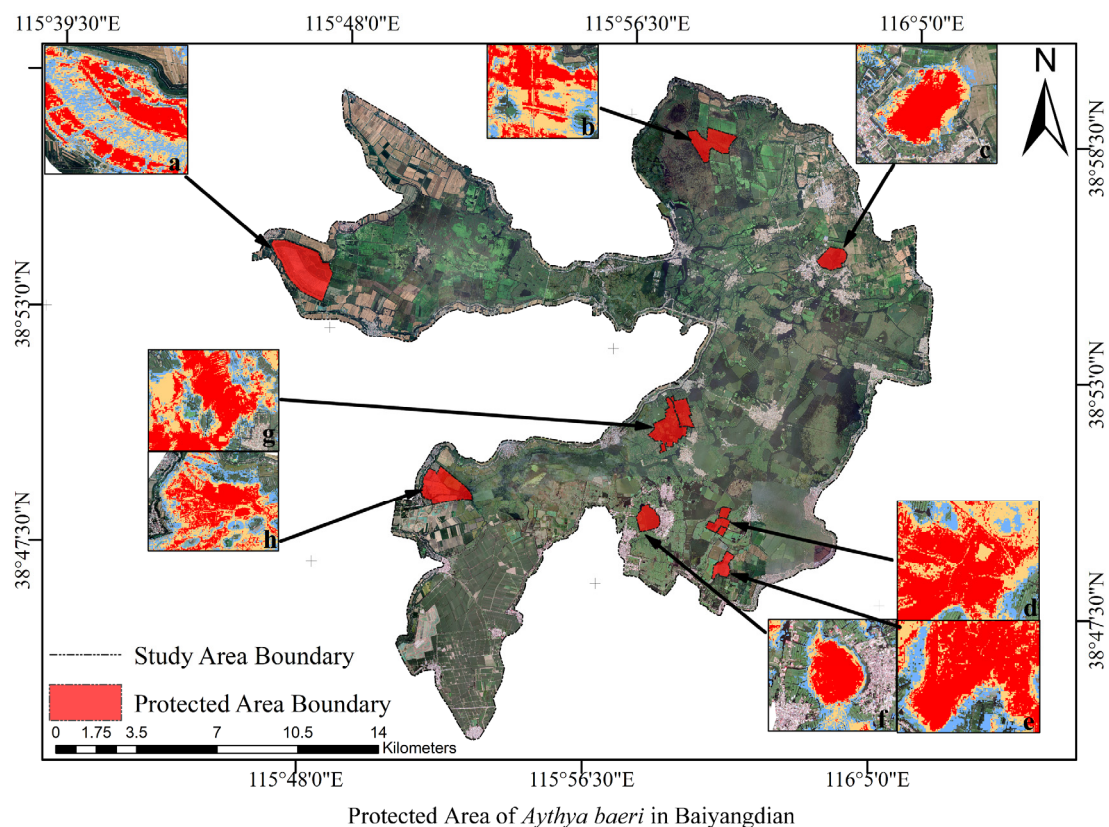


Figure 9. Map of key protection areas for Baer's Pochard in Baiyangdian. The red patches in the map are the protected areas for Baer's Pochard that we proposed. (a) shows the protected area of FHW. (b) shows the protected area of SCD. (c) shows the protected area of JZV. (d) shows the protected area of FYD. (e) shows the protected area of MJD. (f) shows the protected area of DZV. (g) shows the protected area of DTV and BTV. (h) shows the protected area of NQDV.

Our study proposes the following recommendations for the conservation of Baer's Pochard:
 (1) **Formation of Baer's Pochard Conservation Sanctuaries:** Allocate specific areas as dedicated sanctuaries for the Baer's Pochard, focusing on regions with minimal man-

made intrusions. These areas are preferably located within a spatial range of 0.39–0.50 km from the town, less than 0.17 km from open water and less than 1.13 km from the road. In addition, these protected areas should harbor a variety of plant species, including *Potamogeton crispus*, *Nelumbo nucifera*, and *Phragmites australis*. *Nelumbo nucifera* should have a height ranging from 0.2 m to 0.6 m, while *Phragmites australis* should range in height from 2 m to 3.6 m. The water depth within the region should be between 1.5 m and 2.5 m. Large expanses of reed-enclosed paddy fields are recommended within the conservation zones to facilitate Baer's Pochard in evading predators, foraging, and nesting activities. Furthermore, these areas should feature abundant emergent aquatic plants to create a microclimate and maintain localized temperatures during the summer. To safeguard these sanctuaries, stringent regulations on human-driven activities should be enforced, specifically emphasizing a minimum distance of 1.4 km for all waterborne vessels—be it recreational, fishing, or pleasure boats—from these protected environs.

(2) **Augmenting Oversight and Regulatory Measures:** Recognizing the intersection between ideal habitats of Baer's Pochard in BYD and human operations, it is imperative for the relevant authorities to escalate surveillance measures concerning the species. Initiating routine surveys can effectively track the nuanced fluctuations in population metrics. The establishment of a rigorous punitive framework, targeting specifically harmful practices like the employment of toxic bait and electrified fishing prevalent in BYD, is paramount. Robust penalties can serve as effective deterrents against these environmentally harmful actions.

(3) **Advocacy for Conservation Awareness and Community Education:** The effective conservation of vulnerable species mandates a holistic community commitment. Amplifying the public's understanding of avian conservation and the broader ecological framework is of the essence. By fostering a profound emotional resonance and a shared cultural appreciation between the inhabitants and their natural surroundings, conservation goals are more likely to be realized and respected.

5. Conclusions

In our investigation, we amalgamated environmental insights garnered from Sentinel-2 satellite imagery, digital elevation models, human disruption indicators, and the WorldClim bioclimatic variables, employing the GEE for a meticulous analysis of the potential habitats suitable for Baer's Pochard within the BYD terrain. The interplay between various determinants and the selection criteria for suitable habitats by Baer's Pochard was elucidated. Using the MaxEnt model, a comprehensive assessment was undertaken to determine the viable habitats for Baer's Pochard during their breeding and transit phases in BYD. The overarching objective of this study was to provide a well-founded reference that can guide subsequent habitat design, site delineation, and the discernment of habitat variables tailored for Baer's Pochard. Key revelations from the study encompass:

(1) The MaxEnt model served as an efficacious instrument, accurately forecasting the apt habitats for Baer's Pochard across breeding and migratory cycles, thus fortifying its reputation as a dependable predictive mechanism.

(2) The habitat preferences of Baer's Pochard during their reproductive and migratory intervals are driven by an array of elements. Notably, proximity to urban centers and landcover emerged as pivotal influencing factors in the habitat designation process.

(3) A significant recommendation is to advocate for the development of specialized conservation domains for Baer's Pochard in distinct locales like the FHW, the reed-dominant highlands southwest of XBYD, the expansive reed barriers northwest of DTV and BTV, the lotus-rich regions on the eastern flank of SCD's core, and hybrid terrains in JZV's northeastern quadrant where reed-abundant plateaus and man-made fishpond barriers merge. Enhanced surveillance and regulatory regimes are strongly recommended to safeguard these propitious habitats.

To summarize, our study fortifies a robust scientific bedrock that is instrumental in pinpointing and safeguarding viable habitats for Baer's Pochard, which, in turn, has

profound ramifications for bolstering their population metrics and ensuring the species' ecological longevity.

Supplementary Materials: The following supporting information can be downloaded at: <https://www.mdpi.com/article/10.3390/rs16010064/s1>, Figure S1: Correlation analysis of impact factors; Figure S2: Delta.AICc of the different period. Figure S3: Text gain and percent contribution of impact factors in breeding period; Figure S4: Response curves of the main impact factors during the breeding period; Figure S5: Text gain and percent contribution of impact factors in migration period; Figure S6: Response curves of the main impact factors during the migration period. Table S1: Specific area and corresponding percentage of each suitable habitat type for Baer's Pochard during the breeding season. Table S2: Specific area and corresponding percentage of each suitable habitat type for Baer's Pochard during the migratory season.

Author Contributions: Project administration, J.H.; conceptualization, J.H. and Z.T.; investigation, Z.T., D.H., J.Q. and Z.L.; methodology, Z.T.; data curation, D.H.; formal analysis, Z.T.; visualization, Z.T.; writing—original draft, Z.T.; writing—review and editing, K.Y. and J.H. Kunpeng Yi and Jianhua Hou contributed equally to this work. All authors have read and agreed to the published version of the manuscript.

Funding: This research was funded by Research Project on the Breeding Ecology of Baer's Pochard in Baiyangdian under the auspices of the Hebei Xiong'an New Area Management Committee (Grant No. XAXQ-20221225); National Project for the Conservation of Key Bird Species in Baiyangdian, administered by the Hebei Provincial Department of Forestry and Grassland (Grant No. JLC-2021-86); Hebei Natural Science Foundation (Grant No. C2022201042); Collaborative Innovation Center for Baiyangdian Basin Ecological Protection and Beijing-Tianjin-Hebei Sustainable Development; and the National Natural Science Foundation of China (Grant No. 32271674).

Data Availability Statement: The datasets used and analyzed during the current study are available from the corresponding author.

Acknowledgments: We would like to express our gratitude to Jiaojiao Wang and Laikun Ma for their insightful suggestions on manuscript revisions. Special thanks go to Gesang Wangjie for offering valuable input on the experimental design. Furthermore, we acknowledge the invaluable support and assistance provided by Junfeng Yang, Chen Wang, Zongjun Zhang, Wei Liu, Peng Pan, Mengnan Zhang, Jiarong Li, Qi Sun, and Taijun Zuo during the field investigations. Finally, we would like to thank the Xiong'an New Area Administration of Natural Resources and Planning and the Administration of Natural Resources of Anxin County for their support and assistance throughout the course of this study.

Conflicts of Interest: The authors declare no conflict of interest.

References

1. Rands, M.R.W.; Adams, W.M.; Bennun, L.; Butchart, S.H.M.; Clements, A.; Coomes, D.; Entwistle, A.; Hodge, I.; Kapos, V.; Scharlemann, J.P.W.; et al. Biodiversity conservation: Challenges beyond 2010. *Science* **2010**, *329*, 1298–1303. [[CrossRef](#)] [[PubMed](#)]
2. Seto, K.C.; Güneralp, B.; Hutya, L.R. Global forecasts of urban expansion to 2030 and direct impacts on biodiversity and carbon pools. *Proc. Natl. Acad. Sci. USA* **2012**, *109*, 16083–16088. [[CrossRef](#)] [[PubMed](#)]
3. Xie, S.; Su, Y.; Xu, W.; Cai, W.; Wang, X.; Lu, F.; Ouyang, Z. The effect of habitat changes along the urbanization gradient for breeding birds: An example from the Xiong'an New Area. *PeerJ* **2019**, *7*, e7961. [[CrossRef](#)] [[PubMed](#)]
4. Jiang, H.; Wen, Y.; Zou, L.; Wang, Z.; He, C.; Zou, C. The effects of a wetland restoration project on the Siberian crane (*Grus leucogeranus*) population and stopover habitat in Momoge National Nature Reserve, China. *Ecol. Eng.* **2016**, *96*, 170–177. [[CrossRef](#)]
5. Wang, X.; Li, X.; Ren, X.; Jackson, M.V.; Fuller, R.A.; Melville, D.S.; Amano, T.; Ma, Z. Effects of anthropogenic landscapes on population maintenance of waterbirds. *Conserv. Biol.* **2022**, *36*, e13808. [[CrossRef](#)]
6. Liu, J.; Yi, C.; Tang, S.; Zhang, W.; Wen, K.; Qin, C.; Huang, L.; Liu, D.; Jiang, A. Impact of coastal island restoration engineering and subsequent tourism on migratory waterbirds: A 3-year case from Southern China. *Restor. Ecol.* **2023**, *31*, e13974. [[CrossRef](#)]
7. Ning, Y.; Lei, J.; Song, X.; Han, S.; Zhong, Y. Modeling the potential suitable habitat of *Impatiens hainanensis*, a limestone-endemic plant. *Chin. J. Plant Ecol.* **2018**, *42*, 946–954. [[CrossRef](#)]
8. Ye, P.; Zhang, G.; Zhao, X.; Chen, H.; Si, Q.; Wu, J. Potential geographical distribution and environmental explanations of rare and endangered plant species through combined modeling: A case study of Northwest Yunnan, China. *Ecol. Evol.* **2021**, *11*, 13052–13067. [[CrossRef](#)]

9. Brooks, T.M.; Mittermeier, R.A.; Fonseca, G.A.B.; Gerlach, J.; Hoffmann, M.; Lamoreux, J.F.; Mittermeier, C.G.; Pilgrim, J.D. Rodrigues ASL Global biodiversity conservation priorities. *Science* **2006**, *313*, 58–61. [[CrossRef](#)]
10. Zhang, J.; Jiang, F.; Li, G.; Qin, W.; Li, S.; Gao, H.; Cai, Z.; Lin, G.; Zhang, T. Maxent modeling for predicting the spatial distribution of three raptors in the Sanjiangyuan National Park, China. *Ecol. Evol.* **2019**, *9*, 6643–6654. [[CrossRef](#)]
11. Lazo-Cancino, D.; Rivera, R.; Paulsen-Cortez, K.; Gonzalez-Berrios, N.; Rodriguez-Gutierrez, R.; Rodriguez-Serrano, E. The impacts of climate change on the habitat distribution of the vulnerable Patagonian-Fuegian species *Ctenomys magellanicus* (Rodentia, Ctenomyidae). *J. Arid. Environ.* **2020**, *173*, 104016. [[CrossRef](#)]
12. Guisan, A.; Thuiller, W. Predicting species distribution: Offering more than simple habitat models. *Ecol. Lett.* **2005**, *8*, 993–1009. [[CrossRef](#)] [[PubMed](#)]
13. Gobeyn, S.; Mouton, A.M.; Cord, A.F.; Kaim, A.; Volk, M.; Goethals, P.L.M. Evolutionary algorithms for species distribution modelling: A review in the context of machine learning. *Ecol. Model.* **2019**, *392*, 179–195. [[CrossRef](#)]
14. Hao, T.; Elith, J.; Guillera-Arroita, G.; Lahoz-Monfort, J.J. A review of evidence about use and performance of species distribution modelling ensembles like BIOMOD. *Divers. Distrib.* **2019**, *25*, 839–852. [[CrossRef](#)]
15. Phillips, S.J.; Dudík, M. Modeling of species distributions with Maxent: New extensions and a comprehensive evaluation. *Ecography* **2008**, *31*, 161–175. [[CrossRef](#)]
16. Hernandez, P.A.; Graham, C.H.; Master, L.L.; Albert, D.L. The effect of sample size and species characteristics on performance of different species distribution modeling methods. *Ecography* **2006**, *29*, 773–785. [[CrossRef](#)]
17. Pearson, R.G.; Raxworthy, C.J.; Nakamura, M.; Peterson, A.T. Predicting species distributions from small numbers of occurrence records: A test case using cryptic geckos in Madagascar. *J. Biogeogr.* **2007**, *34*, 102–117. [[CrossRef](#)]
18. Zhai, T.; Li, X. Climate change induced potential range shift of the crested ibis based on ensemble models. *Acta Ecol. Sin.* **2012**, *32*, 2361–2370. [[CrossRef](#)]
19. Li, X.; Tian, H.; Yuan, W. Vulnerability of 208 endemic or endangered species in China to the effects of climate change. *Reg. Environ. Change* **2013**, *13*, 843–852. [[CrossRef](#)]
20. Waldrip, S.H.; Niven, R.K. Comparison between Bayesian and maximum entropy analyses of flow networks. *Entropy* **2017**, *19*, 58. [[CrossRef](#)]
21. Phillips, S.J.; Anderson, R.P.; Schapire, R.E. Maximum entropy modeling of species geographic distributions. *Ecol. Model.* **2006**, *190*, 231–259. [[CrossRef](#)]
22. Kumar, L.; Mutanga, O. Google Earth Engine applications since inception: Usage, trends, and potential. *Remote Sens.* **2018**, *10*, 1509. [[CrossRef](#)]
23. Moore, R.; Parsons, E. Beyond SDI, Bridging the Power of Cloud Based Computing Resources to Manage Global Environment Issues. In Proceedings of the INSPIRE Conference, Edinburgh, UK, 27 June–1 July 2011.
24. Gorelick, N.; Hancher, M.; Dixon, M.; Ilyushchenko, S.; Thau, D.; Moore, R. Google Earth Engine: Planetary-scale geospatial analysis for everyone. *Remote Sens. Environ.* **2017**, *202*, 18–27. [[CrossRef](#)]
25. Mutanga, O.; Kumar, L. Google earth engine applications. *Remote Sens.* **2019**, *11*, 591. [[CrossRef](#)]
26. Liu, D.; Zhou, Y.; Fei, Y.; Xie, C.; Hou, S. Mitochondrial genome of the critically endangered Baer’s Pochard, *Aythya baeri*, and its phylogenetic relationship with other Anatidae species. *Sci. Rep.* **2021**, *11*, 24302. [[CrossRef](#)] [[PubMed](#)]
27. Li, C.; Zhang, Y.; Li, J.; Deng, P.; Liu, D.; Zhang, G.; Dong, R. Study on the breeding ecology of *Aythya baeri* in Henan Chenqiao Wetland. *J. Henan Agric. Univ.* **2020**, *54*, 269–275.
28. Wang, X.; Barter, M.; Cao, L.; Lei, J.; Fox, A.D. Serious contractions in wintering distribution and decline in abundance of Baer’s Pochard *Aythya baeri*. *Bird Conserv. Int.* **2012**, *22*, 121–127. [[CrossRef](#)]
29. Hearn, R. The troubled Baer’s Pochard *Aythya baeri*: Cause for a little optimism? *BirdingASIA* **2015**, *24*, 78–83.
30. Chang, Y.; Chang, C.; Li, Y.; Liu, M.; Lv, J.; Hu, Y. Predicting dynamics of the potential breeding habitat of *Larus saundersi* by MaxEnt model under changing land-use conditions in wetland nature reserve of Liaohe Estuary, China. *Remote Sens.* **2022**, *14*, 552. [[CrossRef](#)]
31. Yuan, O.; Liu, S.; Chen, F.; Luo, J.; Hu, H. Habitat suitability evaluation of black-necked cranes based on multi-source remote sensing in Caohai National Nature Reserve, Guizhou. *Acta Ecol. Sin.* **2022**, *42*, 1947–1957.
32. Hou, P.; Bai, J.; Chen, Y.; Hou, J.; Zhao, J.; Ma, Y.; Zhai, J. Analysis on the hotspot characteristics of bird diversity distribution along the continental coastline of China. *Front. Mar. Sci.* **2022**, *9*, 1007442. [[CrossRef](#)]
33. Watson, K.B.; Galford, G.L.; Sonter, L.J.; Ricketts, T.H. Conserving ecosystem services and biodiversity: Measuring the tradeoffs involved in splitting conservation budgets. *Ecosyst. Serv.* **2020**, *42*, 101063. [[CrossRef](#)]
34. Reperant, L.A.; Fučkar, N.S.; Osterhaus, A.D.M.E.; Dobson, A.P.; Kuiken, T. Spatial and temporal association of outbreaks of H5N1 influenza virus infection in wild birds with the 0 C isotherm. *PLoS Pathog.* **2010**, *6*, e1000854. [[CrossRef](#)] [[PubMed](#)]
35. Bai, J.; Yang, Z.; Cui, B.; Gao, H.; Ding, Q. Some heavy metals distribution in wetland soils under different land use types along a typical plateau lake, China. *Soil Tillage Res.* **2010**, *106*, 344–348. [[CrossRef](#)]
36. Xu, M.; Zhu, J.; Huang, Y.; Gao, Y.; Zhang, S.; Tang, Y.; Yin, C.; Wang, Z. The ecological degradation and restoration of Baiyangdian Lake, China. *J. Freshw. Ecol.* **1998**, *13*, 433–446.
37. Yan, S.; Wang, X.; Zhang, Y.; Liu, D.; Yi, Y.; Li, C.; Liu, Q.; Yang, Z. A hybrid PCA-GAM model for investigating the spatiotemporal impacts of water level fluctuations on the diversity of benthic macroinvertebrates in Baiyangdian Lake, North China. *Ecol. Indic.* **2020**, *116*, 106459. [[CrossRef](#)]

38. The Overall Water Quality of Baiyangdian District Has Reached Class III and Entered the Ranks of National Good Lakes. Available online: https://www.gov.cn/xinwen/2022-01/10/content_5667462.htm (accessed on 10 January 2021).
39. Wang, Y.X.; Wang, Y.L.; Han, Y.W.; Li, J. Review of surface water environmental quality standards (2): Introduction and analysis of foreign surface water environmental quality standards and benchmarks. *Sichuan Environ.* **2022**, *41*, 273–280.
40. Li, C.; Cui, H. Evaluation of ecological status and protection countermeasures of Baiyangdian wetland. *J. Agric. Univ. Hebei* **2013**, *15*, 101–104+108.
41. Xing, Y. *Estimation and Analysis of Ecological Service Function Value of Baiyangdian Wetland*; Hebei University: Baoding, China, 2020.
42. Warren, D.L.; Glor, R.E.; Turelli, M. ENMTools: A toolbox for comparative studies of environmental niche models. *Ecography* **2010**, *33*, 607–611. [[CrossRef](#)]
43. Wu, Q.; Wang, L.; Zhu, R.; Yang, Y.; Jin, H.; Zou, H. Nesting habitat suitability analysis of red-crowned crane in Zhalong Nature reserve based on MAXENT modeling. *Acta Ecol. Sin.* **2016**, *36*, 3758–3764.
44. Hao, X.; Wu, Y. Prediction of suitable habitat for overwintering hooded cranes (*Grus monacha*) based on Maxent modeling. *J. Anhui Agric. Univ.* **2017**, *44*, 591–597.
45. Sun, X.; Zhang, Q.; Wu, Q.; Chen, L.; Li, L.; Xu, Z.; Shaliwa, P. Habitat suitability for Bear's Pochard (*Aythya baeri*) in Xianghai Reserve. *J. Northeast. For. Univ.* **2021**, *49*, 112–118.
46. Liu, W.; Hu, C.; Yi, J.; Han, B.; Yu, D.; Xu, H. Status and Distribution of Potential Suitable Habitats of Bear's Pochard Population. *Wetl. Sci.* **2020**, *18*, 387–396.
47. Xia, S.; Hu, D.; Deng, Y.; Zhong, X.; Bai, W.; Zhang, J.; Wang, B.; Zhou, C. Habitat partitioning between sympatric Golden Pheasant and Temminck's Tragopan at different scales. *Acta Ecol. Sin.* **2019**, *39*, 1627–1638.
48. You, Z.; Wang, M.; Lu, B.; Liu, W.; Yang, N. Predicting potential distribution of *Crossoptilon auritum* based on MaxEnt model. *Chin. J. Ecol.* **2022**, *41*, 2271–2277.
49. He, K.; Lei, J.; Jia, Y.; Wu, E.; Sun, G.; Lu, C.; Zeng, Q.; Lei, G. Temporal Dynamics of the Goose Habitat in the Middle and Lower Reaches of the Yangtze River. *Remote Sens.* **2022**, *14*, 1883. [[CrossRef](#)]
50. Radosavljevic, A.; Anderson, R.P. Making better Maxent models of species distributions: Complexity, overfitting and evaluation. *J. Biogeogr.* **2014**, *41*, 629–643. [[CrossRef](#)]
51. Yang, X.Q.; Kushwaha, S.P.S.; Saran, S.; Xu, J.; Roy, P.S. Maxent modeling for predicting the potential distribution of medicinal plant, *Justicia adhatoda* L. in Lesser Himalayan foothills. *Ecol. Eng.* **2013**, *51*, 83–87. [[CrossRef](#)]
52. Morales, N.S.; Fernández, I.C.; Baca-González, V. MaxEnt's parameter configuration and small samples: Are we paying attention to recommendations? A systematic review. *PeerJ* **2017**, *5*, e3093. [[CrossRef](#)]
53. Zhu, G.; Yuan, X.; Fan, J.; Wang, M. Effects of model parameters in MaxEnt modeling of ecological niche and geographic distribution: Case study of the brown marmorated stink bug, *Halyomorpha haly*. *J. Biosaf.* **2018**, *27*, 118–123.
54. Muscarella, R.; Galante, P.J.; Soley-Guardia, M.; Boria, R.A.; Kass, J.M.; Uriarte, M.; Anderson, R.P. ENMeval: An R package for conducting spatially independent evaluations and estimating optimal model complexity for Maxent ecological niche models. *Methods Ecol. Evol.* **2014**, *5*, 1198–1205. [[CrossRef](#)]
55. Phillips, S.J.; Anderson, R.P.; Dudík, M.; Schapire, R.E.; Blair, M.E. Opening the black box: An open-source release of Maxent. *Ecography* **2017**, *40*, 887–893. [[CrossRef](#)]
56. Wang, X.; Duan, Y.; Jin, L.; Wang, C.; Peng, M.; Li, Y.; Wang, X.; Ma, Y. Prediction of historical, present and future distribution of *Quercus sect. Heterobalanus* based on the optimized MaxEnt model in China. *Acta Ecologica Sin.* **2023**, *43*, 6590–6604.
57. Warren, D.L.; Seifert, N.S. Ecological niche modeling in Maxent: The importance of model complexity and the performance of model selection criteria. *Ecol. Appl.* **2011**, *21*, 335–342. [[CrossRef](#)] [[PubMed](#)]
58. Luo, M.; Wang, H.; Lyu, Z. Evaluating the performance of species distribution models Biomod2 and MaxEnt using the giant panda distribution data. *Chin. J. Appl. Ecol.* **2017**, *28*, 4001–4006.
59. Merow, C.; Smith, M.J.; Silander, J.A. A practical guide to MaxEnt for modeling species' distributions: What it does, and why inputs and settings matter. *Ecography* **2013**, *36*, 1058–1069. [[CrossRef](#)]
60. West, A.M.; Kumar, S.; Brown, C.S.; Stohlgren, T.J.; Bromberg, J. Field validation of an invasive species Maxent model. *Ecol. Inform.* **2016**, *36*, 126–134. [[CrossRef](#)]
61. Zhang, Y.; Tang, J.; Ren, G.; Zhao, K.; Wang, X. Global potential distribution prediction of *Xanthium italicum* based on Maxent model. *Sci. Rep.* **2021**, *11*, 16545. [[CrossRef](#)]
62. Liu, C.; Berry, P.M.; Dawson, T.P.; Pearson, R.G. Selecting thresholds of occurrence in the prediction of species distributions. *Ecography* **2005**, *28*, 385–393. [[CrossRef](#)]
63. Ramos, R.S.; Kumar, L.; Shabani, F.; Picanco, M.C. Risk of spread of tomato yellow leaf curl virus (TYLCV) in tomato crops under various climate change scenarios. *Agric. Syst.* **2019**, *173*, 524–535. [[CrossRef](#)]
64. Li, D.; Li, Z.; Liu, Z.; Yang, Y.; Khoso, A.G.; Wang, L.; Liu, D. Climate change simulations revealed potentially drastic shifts in insect community structure and crop yields in China's farmland. *J. Pest Sci.* **2022**, *95*, 55–69. [[CrossRef](#)]
65. He, P.; Li, J.; Li, Y.; Xu, N.; Gao, Y.; Guo, L.; Huo, T.; Peng, C.; Meng, F. Habitat protection and planning for three Ephedra using the MaxEnt and Marxan models. *Ecol. Indic.* **2021**, *133*, 108399. [[CrossRef](#)]
66. Yang, Y.; He, J.; Liu, Y.; Zeng, J.; Zeng, L.; He, R.; Guiang, M.M.; Li, Y.; Wu, H. Assessment of Chinese suitable habitats of *Zanthoxylum nitidum* in different climatic conditions by Maxent model, HPLC, and chemometric methods. *Ind. Crops Prod.* **2023**, *196*, 116515. [[CrossRef](#)]

67. Shi, X.; Wang, J.; Zhang, L.; Chen, S.; Zhao, A.; Ning, X.; Fan, G.; Wu, N.; Zhang, L.; Wang, Z. Prediction of the potentially suitable areas of *Litsea cubeba* in China based on future climate change using the optimized MaxEnt model. *Ecol. Indic.* **2023**, *148*, 110093. [[CrossRef](#)]
68. Amani, M.; Ghorbanian, A.; Ahmadi, S.A.; Kakooei, M.; Moghimi, A.; Mirmazloumi, S.M.; Moghaddam, S.H.A.; Mahdavi, S.; Ghahremanloo, M.; Parsian, S.; et al. Google Earth Engine cloud computing platform for remote sensing big data applications: A comprehensive review. *IEEE Xplore* **2020**, *13*, 5326–5350. [[CrossRef](#)]
69. Canty, M.J.; Nielsen, A.A.; Conradsen, K.; Skriver, H. Statistical analysis of changes in Sentinel-1 time series on the Google Earth Engine. *Remote Sens.* **2020**, *12*, 46. [[CrossRef](#)]
70. Sun, X.; Zhang, Q.; Wu, Q.; Xu, Z.; Deng, W. Suitability evaluation of overwintering habitat for the Bear's Pochard in Henan Minquan wetland park. *J. Northeast. Nor. Univ* **2023**, *55*, 109–113.
71. Wang, B.; Chen, Y.; Lv, C. Evaluating flood inundation impact on wetland vegetation FPAR of the Macquarie Marshes, Australia. *Environ. Earth Sci.* **2015**, *74*, 4989–5000. [[CrossRef](#)]
72. Alibakhshi, S.; Groen, T.A.; Rautiainen, M.; Naimi, B. Remotely-Sensed early warning signals of a critical transition in a wetland ecosystem. *Remote Sens.* **2017**, *9*, 352. [[CrossRef](#)]

Disclaimer/Publisher's Note: The statements, opinions and data contained in all publications are solely those of the individual author(s) and contributor(s) and not of MDPI and/or the editor(s). MDPI and/or the editor(s) disclaim responsibility for any injury to people or property resulting from any ideas, methods, instructions or products referred to in the content.